



Full Text View

[Volume 29, Issue 7 \(July 1999\)](#)

Journal of Physical Oceanography

 Article: pp. 1393–1403 | [Abstract](#) | [PDF \(320K\)](#)

Air Entrainment Processes and Bubble Size Distributions in the Surf Zone

Grant B. Deane

Marine Physical Laboratory, Scripps Institution of Oceanography, University of California, San Diego, La Jolla, California

M. Dale Stokes

Hopkins Marine Station, Stanford University, Pacific Grove, California

(Manuscript received March 6, 1998, in final form June 12, 1998)

DOI: 10.1175/1520-0485(1999)029<1393:AEPABS>2.0.CO;2

ABSTRACT

A new optical instrument was deployed in the surf zone in a trial experiment to measure bubble size distributions and visualize air entrainment and bubble formation mechanisms within breaking surf. Images of bubbles and the evolving air–water mixture inside and beneath breaking wave crests are presented. The images resolve features of the air–water mixture to length scales of hundreds of microns across a 3.7-cm field of view. Two qualitatively different large-scale air entrainment processes are observed. First, intrusions of air and water, thought to be created by jets penetrating the water’s surface, fragment into plumes of bubbles. Second, an air cavity trapped by the overturning wave crest is observed to disintegrate into bubbles. The timescale for the evolution from a compacted air–water mass to individual bubbles was on the order of 90 ms or less for both of these processes. In addition, small-scale air filaments hundreds of microns wide and millimeters long have been discovered beneath wave-induced water jets. The filaments were observed in the process of fragmenting into bubbles hundreds of microns in diameter.

1. Introduction

a. Bubbles in the ocean

Bubbles in the open ocean play an important role in a number of small-scale, upper-ocean physical processes. Physical phenomena affected by the presence of bubbles include enhancement of the air–sea transfer of greenhouse gases at high wind speeds ([Broecker and Siems 1984](#); [Farmer et al. 1993](#); also [Jähne and Monahan 1995](#)), marine aerosol production

Table of Contents:

- [Introduction](#)
- [The bubble imaging instrument](#)
- [Bubble size distributions](#)
- [Images of air entrainment](#)
- [Concluding remarks](#)
- [REFERENCES](#)
- [FIGURES](#)

Options:

- [Create Reference](#)
- [Email this Article](#)
- [Add to MyArchive](#)
- [Search AMS Glossary](#)

Search CrossRef for:

- [Articles Citing This Article](#)

Search Google Scholar for:

- [Grant B. Deane](#)
- [M. Dale Stokes](#)

(Blanchard 1975; Monahan et al. 1986; also Monahan and MacNiocail 1986), optical scattering (Stramski 1994), and the generation of underwater ambient noise (Urick 1986). Oceanic bubbles also contribute to the sea–air flux of moisture and heat (Bortkovskii 1987; Andreas et al. 1995). Bubbles are known to be created in the upper ocean through a variety of mechanisms, such as the action of breaking gravity and capillary waves (see Longuet-Higgins 1993), drop impact on the ocean surface (Franz 1959; Pumphrey and Elmore 1990), and melting snow (Blanchard and Woodcock 1957). However, experiments have shown that under moderate wind conditions, most bubbles near the ocean surface are caused by breaking waves (Koga 1982; Kolovayev 1976; Medwin 1977).

The bubbles entrained by breaking waves are initially packed into plumes, which extend beneath and behind the wave crest. Once created, a bubble plume begins to dissipate through the processes of dissolution, diffusion, and degassing. Large variations in the temporal and spatial distributions of the bubbles occur during this cycle. Void fractions of air in newly created bubble plumes can exceed 50% but the background void fraction between plumes may be many orders of magnitude smaller. The timescales inherent to the different phases of a bubble plume's life cycle also vary greatly, from hundreds of milliseconds during bubble creation to hundreds of seconds for bubble dissolution and degassing. Because of the wide variation in void fractions and timescales associated with the various plume phases, the different phases of a plume's life cycle tend to be treated as separate problems. Monahan (1993) has introduced the terms α plume, β plume, and γ plume to describe the various stages of plume evolution. This paper is concerned with the first second or so of plume formation when the majority of bubbles are created. In Monahan's terminology these are alpha plumes, which persist for a second or so after wave breaking and are characterized by high void fractions (order 1/10 volume ratio of air to water) and a broad spectrum of bubble sizes (millimeters to tens of microns).

b. Bubble size distributions in alpha plumes

There is now a reasonably large body of literature dealing with the distribution of microbubbles in the upper ocean and the physical processes that control their movement and dissolution after creation (see Thorpe 1984). The majority of existing oceanic studies, however, focus on the resident or background population of bubbles rather than the large, transient populations that occur in alpha plumes. Some of the more celebrated studies of resident bubble populations are those of Medwin (1977), Johnson and Cooke (1979), and Kolovayev (1976). Because of the difficulties of making measurements in alpha plumes, which are transient and optically and acoustically opaque, there are few published quantitative studies of their properties. Monahan (1993) has inferred spatially averaged, near-surface bubble size distributions beneath white caps from a sea surface aerosol generation model. Studies of the total void fractions of alpha plumes in the laboratory have been presented by Melville and his coworkers (Lamarre and Melville 1991; Lamarre and Melville 1994; Melville et al. 1993). Deane (1997) has presented measurements, taken from a small sample of photographic images, of the void fraction and distribution of bubble sizes in alpha plumes generated by breaking surf. Here we improve on these results and present further measurements of the bubble size distributions in plumes generated by breaking surf.

c. Air entrainment mechanisms in breaking waves

The physical processes resulting in bubble formation during wave breaking, and their dependence on environmental parameters such as air–sea differential temperature (Hwang et al. 1991), determine the total volume of air entrained and the initial bubble size distribution in alpha plumes. The study of wave-induced bubble formation is intimately related to the fluid dynamics of wave breaking: a complicated subject that is not yet fully understood. However, considerable progress toward elucidating and quantifying the large-scale physical processes occurring in a breaking wave crest has been made in recent years by Melville and others [see Melville (1996) for a review]. In plunging breakers, there are two large-scale flow features that are important to the entrainment of air. These are the jet formed by an overturning wave crest and the water that splashes up from the plunge point where the jet hits the water (Peregrine 1983). In an elegant series of experiments, Bonmarin (1989) used a visualization technique to study the relationship between these flow features and the entrainment of air. Using a high speed movie camera and a stroboscope mounted on a moving carriage, he created images of the shape evolution of a plunging crest after breaking. Bonmarin reported two modes of air entrainment characteristic of plunging breakers. These were the entrainment of air under the falling water jet caused by the overturning wave crest and air entrainment at the point where the falling water jet meets the vortex formed at the rear of the splash-up.

Some air entrainment mechanisms have been proposed. In the Longuet-Higgins and Turner (1974) model for gently spilling breakers, air is mixed with turbulent water spilling over the wave crest. Longuet-Higgins (1992) has also proposed a “crushing air cavity” model for the distribution of bubbles observed immediately after the formation of a bubble plume. The model assumes that the dominant formation process is bubble splitting and is in good agreement with bubble size distributions observed in a variety of naturally occurring settings, including laboratory waves. The physical mechanisms causing bubble splitting, however, are not addressed. One possibility is bubble splitting in convergent and sheared flows, a topic considered by Lewis and Davidson (1982). Other entrainment and bubble creation mechanisms likely to be important in breaking waves are splashes (Franz 1959; Ognz 1997), fluid jets (Koga 1982; Lin and Donnelly 1966; Van De Sande and Smith 1975), and possibly coalescence (Crum 1975; Duineveld 1955; Craig et al. 1993).

Although advances have been made in understanding the large-scale flows in plunging breakers and some theoretical work

has been done on possible bubble formation mechanisms, a detailed physical description of the *small-scale* processes leading to the generation of bubbles within a wave crest remains largely a matter of speculation. One of the main contributions of this work is to present what we believe are the first high resolution images of small-scale bubble formation processes in naturally occurring breaking waves.


2. The bubble imaging instrument

This section contains a description of the new underwater imaging system designed to study alpha plumes. The study of oceanic bubbles using photographic images dates back to the 1970s. [Johnson and Cookes' \(1979\)](#) photographic analysis of bubbles generated in coastal seas by breaking waves is an important and oft-cited work. Although [Medwin \(1977\)](#) is more well known for his various acoustical measurements of oceanic bubble spectra, he obtained one of the earliest photographic results. More contemporary studies include those of Walsh and Mulhearn (1987) and [Wang and Monahan \(1994\)](#). The system described here combines elements of the bubble video microscope described by [Wang and Monahan \(1994\)](#) and the strobed light sheet used by [Bonmarin \(1989\)](#) to visualize breaking waves in the laboratory.

a. The camera

Wave-induced plumes contain bubbles with radii order of centimeters down to tens of microns. The camera described here is not designed to study bubbles over this entire spectrum of length scales but works well for bubbles greater than 200 μm or so in radius. The timescales for deformation of bubbles of this size and larger are sufficiently long to be imaged relatively easily and represent a reasonable first objective for a preliminary, qualitative study of the small-scale dynamics of wave-induced bubble formation processes. To estimate the timescale over which bubble formation may be occurring we need a timescale for bubble deformations. A likely choice is the period of the "breathing mode" oscillations of a newly formed bubble. When a bubble is first formed, it radiates a burst of sound at a frequency approximately given by Minnaert's equation ([Minnaert 1933](#)). A 3.3-mm radius bubble oscillates at 1 kHz at the ocean's surface, with a corresponding timescale of 1 ms. We anticipate that measurements made on millimeter length scales and millisecond timescales will have sufficient spatial and temporal resolution to image bubble formation processes for bubbles a few millimeters in radius and larger. The instrument used in this study was originally designed to measure the evolution of bubble size distributions under breaking waves over roughly 10 seconds, with 90 milliseconds between successive images. The instrument can generate a single image in under a millisecond, which is sufficiently rapid to freeze the bubble formation process.

One of the difficulties of imaging the interior of high void fraction plumes is their dense nature. Bubble creation processes occur in very high void fractions of air, and the air-water mixture is opaque. Both optical and acoustical radiation are strongly scattered at the plume boundaries, making an investigation of the plume's interior with external instruments almost impossible. Our solution to this problem was to design a camera that operates in the plume interior and maintains an optically clear path between the imaging system and the volume under study.

The physics underlying the operation of the camera is the large-angle scattering of light by a bubble. The basic theory for the scattering of light by an air bubble in water was published in the mid-1950s by [Davis \(1955\)](#). The instrument functions by creating a sheet of light, approximately 3.5 mm thick and 37 mm wide, a few millimeters in front of an optical face plate. Bubbles suspended in water within the illuminated volume scatter light out of the sheet and through the optical plate. Bubbles larger than a millimeter or so in radius appear as bright rings when viewed through the face plate. Bubbles smaller than this appear as bright dots. An imaging system (see [Fig. 1](#) ) is housed in a pressure case behind the face plate. The source for the light sheet is a modified commercial camera flash, which provides a burst of light less than a millisecond in duration. The flash tube is held in a mirrored reflector and in front of an optical fiber bundle. The main fiber bundle splits into two smaller bundles, each of which terminates at a cylindrical lens collimator. The light sheets generated by the collimators are directed through the housing face plate onto two 45° mirrors. The mirrors direct the light sheet across the face plate, illuminating the volume of water directly in front of the instrument. An external circular retroreflector surrounds the face plate and mirrors to provide nearly 360° illumination of the water volume.

The imaging system consists of a digital video camera using a progressive scan charge coupled device (CCD) array. The camera provides a composite video output suitable for recording on a video cassette recorder. The progressive scan CCD allows the light integration time of the camera to be controlled in 1/16 000 s increments. The flash unit is synchronized to the video camera with a custom electronics unit. This synchronization, combined with the progressive scan capability of the CCD array, allows "freeze-frame" images to be formed. The digital video camera is coupled into a rod lens optical system (a borescope), which provides a 75° field of view and has a fixed focus from 6 mm to infinity.

b. The action of the camera on locally occurring air entrainment

The imaging instrument affects bubble production because of the proximity of the optical face plate to the water volume being illuminated. The face plate has two effects: it changes the patterns of fluid flow in the local water volume and it presents a barrier to bubbles, which consequently get squashed against the outer edge of the plate. An occurrence of the

latter distortion can be seen in [Fig. 7d](#) —the large region of air in the center of the frame is almost certainly a flattened bubble. Occasionally bubbles adhere to the surface of the face plate, but these are easy to identify as they remain stationary over many frames. Fluid turbulence caused by flow past the retroreflectors and mirrors may cause bubble splitting that would not have occurred in the absence of the instrument.

Notwithstanding effects caused by the presence of the camera, the results from the feasibility study show that useful data can be obtained using our imaging technique. Two large-scale air entrainment processes have been identified in addition to the discovery of small-scale air filaments beneath wave-induced water jets.

3. Bubble size distributions under breaking surf

In this section, bubble size distributions obtained from camera deployments in the surf zone are presented. There are considerable advantages to mounting an experiment in the surf zone over the open ocean. The instrument geometry relative to the breaking waves can be precisely defined, wave breaking patterns are predictable, and the environmental conditions around the measurement site can be easily and accurately monitored. Although air-entrainment processes in the surf zone are of interest in their own right [e.g., see [Peregrine and Thais' \(1996\)](#) treatment of the effect of entrained air in violent water wave impacts], it is relevant to consider how entrainment processes in the surf zone are related to those occurring in the open ocean.

The routes leading to breaking are generally different in the surf zone and the open ocean, but waves in either environment are generally classified as either spilling or plunging [breaking surf is also categorized by [Galvin \(1968\)](#) as surging and collapsing]. Waves in the open ocean may break as a result of constructive interference, wave-wave, wave-current, and wind-wave interactions ([Melville 1996](#)), whereas the route to breaking in the surf zone is generally through shallow water steepening ([Peregrine 1983](#)). Despite the differences in the mechanisms inducing wave breaking, there is evidence to support the hypothesis that the underlying bubble formation processes are similar. [Koga \(1982\)](#) has studied bubble formation mechanisms in wind-induced spilling breakers in the laboratory and describes lines of bubbles where bubble clusters and large bubbles occur. These features are the result of an intermittent entrainment mechanism ([Koga 1982](#)) and are qualitatively similar to the plumes of bubbles observed under spilling breakers in the surf zone.

a. The deployment geometry

A schematic of the deployment geometry for the surf zone experiment is shown in [Fig. 2](#). The instrument was deployed in the surf zone off La Jolla Shores Beach at two heights and under breaking waves of order 15-cm height. The two deployment heights were level with the breaking wave crest and roughly 5 cm below the mean water surface, respectively labeled location I and location II in [Fig. 2](#). Deployment location I yielded images of processes occurring in the crest itself, and these results are described in [section 4](#). Location II showed patterns of plume creation and also yielded a time series of the bubble size distribution at a fixed location in the water column. The long axis of the camera was held parallel to the seafloor and perpendicular to the direction of the wave motion. The net effect was for waves to pass along the front of the optical face plate from left to right. The camera light sheet was flashed every 90 milliseconds, resulting in a sampling frequency of just over 10 Hz. The camera's electronic shutter speed was set to 1/1000 s, which was sufficient to freeze the motion of the bubbles. The resulting images span 3.7 cm and resolve features on a spatial scale of around 100 μm .

b. Images and size distributions

Two images of bubbles inside an alpha plume, taken immediately after the passage of a breaking wave crest over the camera, are shown in [Fig. 3](#). The camera was held approximately 5 cm below the mean water level, at location II in [Fig. 2](#). The borescope attached to the camera forms circular images approximately 3.7 cm in diameter, and the black areas in the images correspond to regions that lie outside the borescope's field of view. The bright circles and dots in the illuminated region were caused by air bubbles caught in the light sheet as the instrument flashed (see [section 2](#) for a detailed description of the camera's operation).

The size of individual bubbles can be estimated by electronic processing of the digitized camera image. The full details of the processing scheme will be discussed in greater detail in a later paper. For our present purposes, it is sufficient to say that the automated processing algorithm counts bubbles of a given radius using a modified circular Hough transform. This technique is a robust method of shape analysis used to detect circular objects. When applied to the images of bubbles, the algorithm returns the center coordinates and radii of all the bubbles lying between specified radii. This information is sufficient to compute the bubble density in units of bubbles per cubic meter per micron of bubble radius increment at the instant that the image was formed. The bubble radius increment used for the analysis was chosen to coincide with the pixel resolution of the image, which was approximately 78 μm . The resulting distribution represents an average over the sampling volume of the camera, which is approximately 3.7 cm³.

The time evolution of the bubble size distribution at a fixed location can be determined by applying the bubble counting

technique described above to a sequence of images. The bubble density estimates resulting from an analysis of 19 consecutive images taken immediately after a breaking wave crest passed over the camera are plotted in [Fig. 3](#) as a function of bubble radius and time. Immediately after formation, bubble plumes are advected through the water column in the direction of the wave motion. Consequently, the temporal variations seen in the bubble size distribution at the (fixed) camera location are a superposition of temporal and spatial gradients in the bubble field and do not represent the changing bubble size distribution in a *single* plume. Advection of bubbles past the camera is particularly evident in the fluctuations of the size distribution approximately one second into the data record.

The bubble size distribution obtained by averaging the record shown in [Fig. 3](#) is plotted in [Fig. 4](#). The squares are the data points obtained from the present study and the circles and straight lines respectively are data points and a scaling law from an earlier optical study of the bubble size distribution of alpha plumes in the surf zone ([Deane 1997](#)). The data points from the earlier study have been halved in radius to correct a scaling error in the published curve. The present result is in reasonable agreement with the earlier distribution, the two differing by no more than a factor of 3 across the spectrum.

4. Images of air entrainment mechanisms from the surf zone

a. The deployment geometry

The results presented in this section were obtained from a preliminary experiment to study the feasibility of using the bubble-counting camera to visualize air-entrainment mechanisms. The camera was deployed in gently spilling breakers in the surf zone to obtain images of the evolving air-water mixture during the process of plume creation.

b. Air entrainment by turbulent jets

[Figure 5a](#) shows an image taken approximately 5 cm below the mean water surface during a breaking event (location II in [Fig. 2](#)). Light is scattered into the camera from air-water boundaries. The images that precede [Fig. 5a](#) indicate that the camera was below the mean water surface when the light sheet flashed. It follows that the bright features in the image are the boundaries of air cavities. There are two spearlike shapes extending horizontally across the image, which, anticipating our later interpretation, have been labeled “jet intrusions.” The degree of contrast in the image indicates that only the bright, right-hand end of the upper intrusion is in the light sheet in front of the face plate; the rest of the image is formed from reflections of stray light, which is either diverging from or scattered out of the light sheet. A tentative interpretation of the bubble creation processes occurring at the time of the image can be formed from the patterns of air distribution apparent in the intrusions. The interpretation is based on the two regions of the intrusions within the white squares labeled I and II in [Fig. 5a](#).

The boundary of the intrusion illuminated inside region I is made of small, coherent cavities of air compacted together. We have labeled these features “filaments” because of their apparent strandlike nature. The filaments are a few hundred microns across and would be millimeters long if stretched out. The filament at the bottom of the region, labeled “filament sheet,” has the appearance of maintaining a continuous boundary, which extends back into the image. It is not possible to say from the image if the other filaments maintain a coherent structure below the illuminated surface. Small, coherent structures like these are reminiscent of the sheath of air created by a plunging, laminar liquid jet ([Lin and Donnelly 1966](#); [McKeogh and Irvine 1981](#)). Such structures are not expected to be stable, and there is evidence in region II that the ultimate fate of the filaments is to fragment into small bubbles.

Region II shows the left-hand end of the upper intrusion fragmenting into air bubbles several hundred microns and smaller in diameter. Although there is no direct evidence that the bubbles are the product of fragmenting filaments, there are features in the region that could be interpreted as filament remnants.

[Figure 6](#) shows juxtaposed images of the jet intrusions and an image taken 90 milliseconds later. The complicated, coherent features of the jet intrusions have been replaced by a cloud of bubbles that range in radius from hundreds of microns to several millimeters. Evidently, the bubbles are the debris of the intrusions, which took 90 milliseconds or less to fragment. Analysis of the complete video sequence indicates that the net water flow at the time of the images was toward, rather than across, the camera.

c. The crushing of an air cavity

By “air cavity,” we mean the pocket of air trapped between the breaking wave crest and ocean surface (see [Fig. 7b](#)). [Figure 7](#) shows six frames taken during a breaking event roughly at the height of the wave crest (location I of [Fig. 2](#)). The first frame shows the air-laden water of the breaking wave crest approaching from the left. The optical system is sufficiently sensitive to form images from the ambient light field at the short shutter speeds, and the sky and the La Jolla Shores cliffs are visible in the background. The bright stripe in the top, left-hand corner of frames 7a and 7b is a spurious

reflection from one of the 45° mirror reflectors. In frame 7b, the wave crest has moved over the instrument and the image shows the air cavity created by the ocean surface and the overturning crest. The remaining images show the evolving air–water mixture left behind the wave.

There is a clear evolution from the air cavity in frame 7b to the individual bubbles in frame 7f. Some bubbles can be seen in frame 7c, but most of the air is packed into a complicated, almost continuously connected mass. The image taken 90 milliseconds later shows mostly bubbles interspersed among a few centimeter scale air masses, showing that the complicated air–water mixture in frame 7c has evolved into bubbles during the delay between the images. It was during this time that the majority of bubble creation events occurred. Frames 7e and 7f respectively show fewer and smaller bubbles as buoyancy removed many of the larger bubbles from the imaging volume, but little evidence of significant bubble formation activity. A few of the bubbles in frames 7d and 7e are highly deformed and appear to be in the process of splitting.



d. Advection

There are two methods for interpreting the images generated by the instrument. First, we can examine the patterns of the air–water boundaries in individual images, which yield a “snapshot” of bubble formation. The second method is to study the differences between images, which gives a dynamical view of the evolving air–water mixture. The problem with the dynamical analysis is that, unless successive images are taken on sufficiently short timescales, there is an ambiguity between changes caused by temporal evolution and advection of the water mass past the imaging instrument. In order to unambiguously distinguish between temporal and material derivatives, individual features need to be tracked, which would require a reduction in the delay between images from 90 milliseconds to millisecond timescales.


The measurements reported here were made in a water depth of approximately $h = 30$ cm, implying a linear, shallow water wave speed of roughly $c = (gh)^{1/2} \approx 1.7 \text{ m s}^{-1}$, where $g = 9.8 \text{ m s}^{-2}$ is the acceleration due to gravity. This speed implies that the breaking wave crest is translated horizontally by 15 cm between successive images, which is four times the camera’s field of view. The alpha plumes created by the breaking crest are initially advected in the direction of wave motion with some finite fraction of the crest speed and successive images formed during the passage of the wave over the camera will almost certainly be affected by advection.

5. Concluding remarks

The images obtained in the trial deployment illustrate the potential for visualizing bubble formation processes in breaking waves. The data show evidence of two large-scale mechanisms causing air entrainment: jet intrusions and the crushing of air cavities. These mechanisms are consistent with the results from [Bonmarin’s \(1989\)](#) flow visualization studies. The air cavity is the feature Bonmarin identifies as the air entrapped under the falling water jet, and is well known to lead to bubble formation in plunging breakers ([Melville 1996](#)). A reasonable explanation for the structures we have called “jet intrusions” is that they are caused by entrance of the falling jet into the front of the wave.

In addition, two small-scale bubble formation processes have been observed. The first of these is the unstable breakup of filaments of air some hundreds of microns wide and millimeters long, shown in [Fig. 5a](#) . The physics of this process may be similar to the unstable breakup of the thin shell of gas formed around a laminar liquid jet as it penetrates into liquid. The second process is the splitting of large bubbles, which is inferred from the images of highly deformed bubbles in [Figs. 7d and 7e](#) .

The processes leading to bubble formation by the jet intrusions and the crushing of the air cavity took place in the time interval between two successive images, or 90 ms. The implication is that the majority of bubbles in alpha plumes are formed on quite short timescales compared with the lifetime of the plume. This observation is in agreement with results from an acoustic experiment to measure the sound of breaking surf ([Deane 1997](#)), which provided evidence for episodic bursts of bubble creation lasting 50 ms or so.

Based on the evidence from the trial deployment and study of the relevant literature, a plausible sequence of events leading to bubble formation is as follows. Immediately before a wave breaks, an overturning jet is formed at the top of the wave crest. The jet is a feature common to both spilling and plunging breakers ([Longuet-Higgins and Cokelet 1978](#)), differing only in the local scale ([Longuet-Higgins 1987](#)). As the jet forms, it may become turbulent, entraining air before impacting on the ocean surface. Once the air-laden jet impacts the forward surface of the wave crest, additional entrainment occurs at the entry point, forming the jet intrusions illustrated in [Fig. 5a](#) . The observed jet intrusions were centimeters long and were at least partly composed of thin filaments of air, several hundred microns wide and millimeters in length. The small-scale filaments appear to be unstable, and fragment into submillimeter-sized bubbles.

In addition to jet intrusions, a cavity of air is trapped by the overturning wave crest. The air cavity is ultimately broken up into small bubbles, possibly through the splitting of bubbles in turbulent and sheared flow. In the first second of breaking, these processes result in one or more high void fraction bubble plumes beneath the wave. While the void fraction is high,

bubble coalescence may play a role in creating new bubbles from air already entrained in the water column.

Acknowledgments

We are pleased to thank Prof. Michael Longuet-Higgins and Prof. Michael Buckingham for their comments and Mr. James Uyloan for his assistance with the camera construction and deployment. We are grateful to two anonymous reviewers who suggested significant improvements to the manuscript. This work was supported by Office of Naval Research Contract N00014-96-0297.

REFERENCES

- Andreas, E. L., J. B. Edson, E. C. Monahan, M. P. Rouault, and S. D. Smith, 1995: The spray contribution to net evaporation from the sea: A review of recent progress. *Bound. Layer Meteor.*, **72**, 3–52..
- Blanchard, D. C., 1975: Bubble scavenging and the water-to-air transfer of organic material in the sea. *Adv. Chem. Ser.*, **145**, 360–387..
- , and A. H. Woodcock, 1957: Bubble formation and modification in the sea and its meteorological significance. *Tellus*, **9**, 145–158..
- Bonmarin, P., 1989: Geometric properties of deep-water breaking waves. *J. Fluid Mech.*, **209**, 405–433..
- Bortkovskii, R. S., 1987: *Air–Sea Exchange of Heat and Moisture during Storms*. Kluwer Academic, 194 pp..
- Broecker, H. C., and W. Siems, 1984: The role of bubbles in gas transfer from water to air at higher windspeeds. *Gas Transfer at Water Surfaces*, Reidel, 639 pp..
- Craig, V. S. J., B. W. Ninham, and R. M. Pashley, 1993: The effect of electrolytes on bubble coalescence in water. *J. Phys. Chem.*, **97**, 10 192–10 197..
- Crum, L. A., 1975: Bjerknes forces in a stationary sound field. *J. Acoust. Soc. Amer.*, **57**, 1363–1370..
- Davis, G. E., 1955: Scattering of light by an air bubble in water. *J. Opt. Soc. Amer.*, **45**, 572–581..
- Deane, G. B., 1997: Sound generation and air entrainment by breaking waves in the surf zone. *J. Acoust. Soc. Amer.*, **102**, 2671–2689..
- Duineveld, P. C., 1995: Bouncing and coalescence of two bubbles in pure water. *Liquid/Gas and Liquid/Vapor Two-Phase Systems*, S. Morioka and L. van Wijngaardeng, Eds., Kluwer Academic..
- Farmer, D. M., C. L. McNeill, and B. D. Johnson, 1993: Evidence for the importance of bubbles in increasing air–sea gas flux. *Nature*, **361**, 620–623..
- Franz, G. J., 1959: Splashes as sources of sound in liquids. *J. Acoust. Soc. Amer.*, **31**, 1080–1096..
- Galvin, C. J., Jr., 1968: Breaker type classification on three laboratory beaches. *J. Geophys. Res.*, **73**, 3651–3659..
- Hwang, P. A., Y. Poon, and J. Wu, 1991: Temperature effects on generation and entrainment of bubbles induced by a water jet. *J. Phys. Oceanogr.*, **21**, 1602–1605.. [Find this article online](#)
- Jähne, B., and E. C. Monahan, Eds., 1995: *Air–Water Gas Transfer: Selected Papers from the Third International Symposium on Air–Water Gas Transfer*. Aeon Verlag, 900 pp..
- Johnson, B. D., and R. C. Cooke, 1979: Bubble populations and spectra in coastal waters: A photographic approach. *J. Geophys. Res.*, **84**, 3761–3766..
- Koga, M., 1982: Bubble entrainment in breaking wind waves. *Tellus*, **34**, 481–489..
- Kolovayev, P. A., 1976: Investigation of the concentration and statistical size distribution of wind-produced bubbles in the near-surface ocean layer. *Oceanology* (English translation), **15**, 659–661..
- Lamarre, E., and W. K. Melville, 1991: Air entrainment and dissipation in breaking waves. *Nature*, **351**, 469–472..
- , and —, 1994: Void fraction measurements and sound-speed fields in bubble plumes generated by breaking waves. *J. Acoust. Soc. Amer.*, **95**, 1317–1328..

Lewis, D. A., and J. F. Davidson, 1982: Bubble splitting in shear flow. *Trans. Inst. Chem. Eng.*, **60**, 283–291..

Lin, T. J., and H. G. Donnelly, 1966: Gas bubble entrainment by plunging laminar liquid jets. *Amer. Inst. Chem. Eng.*, **12**, 563–571..

Longuet-Higgins, M. S., 1987: Mechanisms of wave breaking in deep water. *Sea Surface Sound. Natural Mechanisms of Surface Generated Noise in the Ocean*, B.R. Kerman, Ed., Kluwer Academic, 1–30..

—, 1992: The crushing of air cavities in a liquid. *Proc. Roy. Soc. London A*, **439**, 611–626..

—, 1993: Bubble noise mechanisms—A review. *Natural Physical Sources of Underwater Sound*, B. R. Kerman, Ed., Kluwer Academic, 419–452..

—, and J. S. Turner, 1974: An “entraining plume” model of a spilling breaker. *J. Fluid Mech.*, **63**, 1–20..

—, and E. D. Cokelet, 1978: The deformation of steep surface waves on water. Part II: Growth of normal mode instabilities. *Proc. Roy. Soc. London A*, **364**, 1–28..

McKeogh, E. J., and D. A. Ervine, 1981: Air entrainment rate and diffusion pattern of plunging liquid jets. *Chem. Eng. Sci.*, **36**, 1161–1172..

Medwin, H., 1977: In situ acoustic measurements of microbubbles at sea. *J. Geophys. Res.*, **82**, 971–976..

Melville, W. K., 1996: The role of surface-wave breaking in air–sea interaction. *Annu. Rev. Fluid Mech.*, **28**, 279–321..

—, M. R. Loewen, and E. Lamarre, 1993: Bubbles, noise and breaking waves: A review of laboratory experiments. *Natural Physical Sources of Underwater Sound*, B. R. Kerman, Ed., Kluwer Academic, 483–501..

Minnaert, M., 1933: On musical air bubbles and the sounds of running water. *Philos. Mag.*, **16**, 235–248..

Monahan, E. C., 1993: Occurrence and evolution of acoustically relevant sub-surface bubble plumes and their associated, remotely monitorable, surface whitecaps. *Natural Physical Sources of Underwater Sound*, B. R. Kerman, Ed., Kluwer Academic, 503–517..

—, and G. MacNiocaill, Eds., 1986: *Oceanic Whitecaps and Their Role in Air–Sea Exchange Processes*. Kluwer Academic, 294 pp..

—, D. E. Speil, and K. L. Davidson, 1995: A model of marine aerosol generation via whitecaps and wave disruption. *Oceanic Whitecaps and Their Role in Air–Sea Exchange Processes*, E. C. Monahan and G. MacNiocaill, Eds., Kluwer Academic..

Ognz, H. N., 1997: Air entrainment upon liquid impact. *Philos. Trans. Roy. Soc. London A*, **355**, 491–506..

Peregrine, D. H., 1983: Breaking waves on beaches. *Annu. Rev. Fluid Mech.*, **15**, 149–178..

—, and I. Thais, 1996: The effect of entrained air in violent water wave impacts. *J. Fluid Mech.*, **325**, 377–397..

Pumphrey, H. C., and P. A. Elmore, 1990: The entrainment of bubbles by drop impacts. *J. Fluid Mech.*, **220**, 539–567..

Stramski, D., 1994: Gas microbubbles: An assessment of their significance to light scattering in quiescent seas. *The International Society for Optical Engineering*, J. S. Jaffe, Ed., International Society for Optical Engineering, 704–710..

Thorpe, S. A., 1984: A model of the turbulent diffusion of bubbles below the sea surface. *J. Phys. Oceanogr.*, **14**, 841–854.. [Find this article online](#)

Urlick, R. J., 1986: *Ambient Noise in the Sea*. Peninsula Publishing, 205 pp..

Van De Sande, E., and J. M. Smith, 1975: Jet break-up and air entrainment by low velocity turbulent water jets. *Chem. Eng. Sci.*, **31**, 219–224..

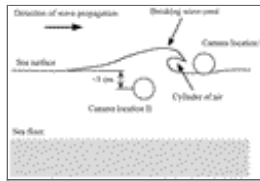
Wang, Q., and E. C. Monahan, 1994: The influence of salinity on the spectra of bubbles formed in breaking wave simulations. *Sea Surface Sound '94*, M. J. Buckingham and J. R. Potter, Eds., World Scientific, 312–319..

Figures



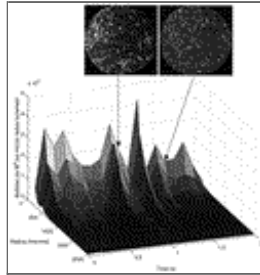
Click on thumbnail for full-sized image.

Fig. 1. The optical imaging instrument. The diagram is approximately to scale and the diameter of the pressure housing is 11.4 cm.



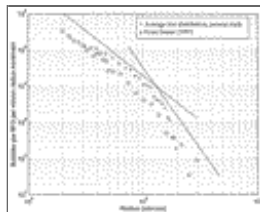
Click on thumbnail for full-sized image.

Fig. 2. The deployment geometry for the visualization of breaking surf. Location I provided images of processes occurring within the breaking wave crest. Location II provided images of jet intrusions and the bubble size distribution in alpha plumes.



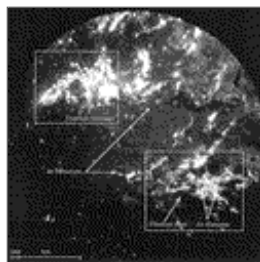
Click on thumbnail for full-sized image.

Fig. 3. Images of bubbles in the water column approximately 1 s after the passage of a breaking wave crest over the camera. The surface plot shows an analysis of 19 images into estimates of the bubble size distribution as a function of bubble radius and time.



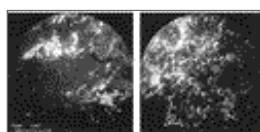
Click on thumbnail for full-sized image.

Fig. 4. The bubble size distribution obtained by averaging the 19 separate distributions plotted in Fig. 3. The crosses are the number density estimates from the present study, the circles the (corrected) bubble size distribution from Deane (1997). The solid lines are the size distribution from Eq. (9) of Deane (1997) reproduced for comparison.



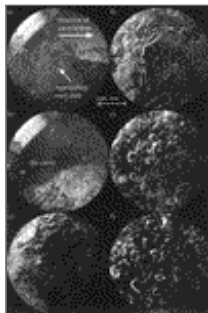
Click on thumbnail for full-sized image.

Fig. 5. Spearlike intrusions of air caused by a wave breaking overhead. The smallest discernable features in the image are several hundred microns in length. Region I: The air cavity in this region consists of small, coherent structures several hundred microns wide and millimeters in length. Region II: The air cavity is fragmenting into numerous bubbles hundreds of microns and smaller in diameter.



Click on thumbnail for full-sized image.

Fig. 6. Juxtaposed images of the jet intrusions and an image taken 90 milliseconds later. Evidently, the jet intrusions have fragmented into a plume of bubbles. Analysis of the complete video sequence indicates that the net water flow at the time of the images was toward, rather than across, the camera.



[Click on thumbnail for full-sized image.](#)

Fig. 7. Images taken in a breaking wave crest showing the crushing of an air cavity. Successive images were taken every 90 milliseconds. (a) The approaching wave crest. (b) The air cavity trapped by the overturning wave crest. (c)–(f) The evolving air–water mixture behind the wave crest.

Corresponding author address: Dr. Grant B. Deane, Scripps Institution of Oceanography, Mailcode 238, Marine Physical Lab., University of California, San Diego, La Jolla, CA 92093-0238.

E-mail: grant@mpl.ucsd.edu

[top ▲](#)



© 2008 American Meteorological Society [Privacy Policy and Disclaimer](#)
Headquarters: 45 Beacon Street Boston, MA 02108-3693
DC Office: 1120 G Street, NW, Suite 800 Washington DC, 20005-3826
amsinfo@ametsoc.org Phone: 617-227-2425 Fax: 617-742-8718
[Allen Press, Inc.](#) assists in the online publication of *AMS* journals.